A method for the correction of size effects in microparticles using a peak-to-background approach in electron-probe microanalysis

Mouad Essani, Emmanuelle Brackx, Emmanuel Excoffier

Version of Record: https://www.sciencedirect.com/science/article/pii/S0584854720301300
Manuscript_6fa39649ed426377974046ef575fa604

A method for the correction of size effects in microparticles using a peak-to-background approach in electron-probe microanalysis

Mouad Essani[1,2,*], Emmanuelle Brackx[1], and Emmanuel Excoffier[1]

[1]CEA, DEN, DMRC, Univ Montpellier, Marcoule, France

[2]Sorbonne Université, CNRS UMR 7614, Laboratoire de Chimie Physique- Matière et Rayonnement, 4 Place Jussieu, F-75252 Paris Cedex 05, France

Abstract: We describe a correction method in electron probe microanalysis (EPMA) for size effects in microparticles. Accounting for size effects is important in quantitative EPMA of microparticles, where bulk standards are usually used for quantification. In this work, the correction was applied using peak-to-background ratios $\left(\frac{P}{B}\right)$ that are quasi-independent of absorption path lengths, which enables the difference in absorption between a microparticle and a bulk sample to be taken into account. For microparticles smaller than the X-ray generation volume, the X-ray emission inside the particle can be significantly affected by the transmission of electrons through the particle, thus requiring a correction in the measured $\frac{P}{B}$ ratios. Moreover, transmitted electrons induce Bremsstrahlung from the substrate that can also affect the $\frac{P}{B}$ ratios. This raises the necessity to include a correction of the substrate emission in the $\frac{P}{B}$ methods applied for microparticles. The present method enables to correct for the effects due to electron transmission as well as the parasitic emission of the substrate. In order to assess the validity of our method, the corrected $\frac{P}{B}$ of small particles were compared with those obtained for a bulk sample or a pseudo-bulk particle where size effects are negligible. Corrected $\frac{P}{B}$ were further used in a ZAF $\frac{P}{B}$ method [J. Lábár, S. Török, X-Ray Spectrom. 21 (1992) 183–190] to evaluate the correction model in terms of quantitative analysis. The study was performed on homogeneous spherical microparticles of K411 glass and microparticles of UO_2. Both substrate and transmission effects were taken into account in the K411 glass particles, which led to significant improvements in terms of quantitative results. For UO_2 particles, size effects did not have much impact on the $\frac{P}{B}$ ratios and accurate quantification was obtained from both uncorrected and corrected ratios.

Keywords Electron probe microanalysis. Microparticles. Peak-to-background method. X-ray emission

INTRODUCTION

Electron probe microanalysis is one of the most widely-used non-destructive techniques for the quantification of solid samples. The quantitative analysis is usually performed using bulk polished standard samples, where the X-ray characteristic intensity $I^i{}_{sample}$ emitted from the element i of the sample being analyzed is compared to the intensity $I^i{}_{standard}$ emitted from the same element of the standard. The concentration C_i can be further determined by means of the k-ratio, $k_i = \frac{I^i{}_{sample}}{I^i{}_{standard}}$, to which a conventional **ZAF** or $\varphi(\rho z)$ method [1, 2] is applied for the correction of matrix effects, i.e. effects related to atomic number (**Z**), absorption (**A**), and fluorescence (**F**).

Quantification based on standards usually requires both the sample studied and the standard to be analyzed under the same experimental conditions. Moreover, a sample preparation step is often necessary in order to reduce inaccuracies due to the geometric effects that have an impact on the X-ray emission inside the specimen.

The quantification of powder composed of microparticle assemblies is a special example, requiring a preparation step where the powder is embedded inside a resin and polished before the analysis [3]. Other than being time consuming, the polishing procedure may induce defects in the sample, for example surface contamination [4,5]. Moreover, it is often important to know whether a powder manufacturing protocol produces a homogeneous stoichiometry and composition, or if the elements of a geological powder are homogeneously distributed. This information can only be gained reasonably accurately if the powder analysis is performed on each individual particle.

On the other hand, quantifying the powder without a preparation step can have a major impact on the accuracy of quantitative results. This is mainly due to absorption and geometrical effects inside the microparticles that are not properly corrected by the ZAF models based on bulk polished standards.

Many attempts have been made to adjust models based on bulk standards for microparticle analysis. Armstrong developed a particle-ZAF algorithm in which a bulk depth distribution of X-ray intensities ($\varphi(\rho z)$) was integrated over the volume of the particle [6]. Despite its success, the model does not consider the effects of the incidence angle and radial distribution of X-ray emission, and only deals with cases where particles are analyzed with an electron beam at normal incidence.

Another issue that is often encountered when dealing with microparticles is the emission of X-rays from the substrate [7,8]. This originates from energetic electrons that leave the microparticle (through side scattering or transmission) and excite the substrate atoms. The substrate emission induces the detection of parasitic signals that may lead to false estimations of the particle chemical composition.

In some cases, particles can exhibit surface roughness and complex morphology, which makes it even more complicated to provide suitable standard samples. These issues make the quantification of microparticles even more complicated and very challenging.

An approach used by many authors when considering the loss of intensity due to absorption, and surface roughness is the peak-to-background ($\frac{P}{B}$) method [9-12]. The assumption that the depth distributions of both characteristic and continuum radiation are similar, which is a reasonable consideration in a narrow energy band, guarantees the independence of their ratio $\frac{P}{B}$ with respect to electron incidence angle and absorption path length. In addition, instrumental parameters are not required in $\frac{P}{B}$ based methods as they allow compensation for multiple uncertainties. Accurate results have been obtained in a number of quantification procedures based on $\frac{P}{B}$ ratios [13,14].

In this work, we describe a correction of size effects for $\frac{P}{\mathrm{B}}$ ratios that could be useful in the quantitative X-ray microanalysis of microparticles. A study was performed on NIST (National Institute of Standards) spherical microparticles of K411 glass and on microparticles of UO_2. Different particle sizes were studied and those chosen were less than 3 µm. In order to investigate the influence of the substrate emission, a further study was carried out on particles deposited on four different substrates of B_4C, Al, Ni and W. We suggest the correction of two main effects that can have an impact on the $\frac{P}{\mathrm{B}}$ ratios of small particles, which are the loss due to electron transmission and substrate

effects. The applicability of our correction model for quantitative analysis was further tested by using it in the Lábár and Török ZAF $\frac{P}{B}$ method.

EXPERIMENTAL SECTION

Measurements. X-ray intensities were measured on a Merlin field-emission scanning electron microscope equipped with an Oxford energy dispersive spectrometer positioned at a take-off angle of ~35° from the sample. The spectrometer has a silicon drift detector and an AP3 Moxtek window supported by a rigid silicon grid. In order to collect a maximum number of emitted photons and minimize uncertainties, the distance between the spectrometer and the sample was set at 19.5 mm.

All measurements were performed using the longest shaping time and an electron probe current of 0.1 nA~0.2 nA, so as to obtain a resolution of 125 eV FWHM at Mn Kα and a counting rate that did not exceed 30% in dead time. The uncertainties associated with the counting statistics were generally within 1-2% for characteristic lines and ranged from 4 to 8% for the background intensities. The precision in determining the number of incident electrons was estimated to be about 2% using a Faraday cup.

Determination of Bremsstrahlung intensities. Experimental Bremsstrahlung intensities under characteristic lines were determined after adjusting the background of each measured spectrum. The adjustment was based on a method similar to the one described by Trincavelli et al [14], where the measured continuum is corrected and fitted using a non-linear least square method. Characteristic, escape, and pile-up peaks were removed from the measured spectra. The resulting spectrum was afterward corrected for absorption, detection efficiency and backscattering effects in order to obtain Bremsstrahlung intensities generated in the sample.

The modified Philibert's absorption factor [15] was used to account for absorption correction. Mass absorption coefficients used in this work are those tabulated by Henke et al. [16]. Backscattering loss corrections were carried out using Statham's formula [17]:

$$R = 1 - (1 - R_c)\left(\frac{2}{1+\eta}\right)^{0.63}\left(0.79 + \frac{0.44\,E}{E_0}\right) \quad (1)$$

with η the backscattering coefficient [18] and R_c the backscattering correction factor for characteristic radiation given by Love et al. [18]:

$$R_c = 1 - \eta\,[I(U_0) + \eta\,G(U_0)]^{1.67} \quad (2)$$

where I and G are function of the overvoltage $U_0 = E_0/E$. The Bremsstrahlung intensities I_{bg} were further corrected for the loss caused by the detection efficiency. Since the thicknesses of layers of polymer, DuraCoat™, and aluminum in the spectrometer window were not known with sufficient accuracy, the conventional EDS efficiency equation [19] could not be used. Instead, the method proposed by Merlet et al. [20] was implemented, in which the total detector efficiency is given as the ratio between the measured Bremsstrahlung intensities and those obtained by Monte Carlo (MC) simulations:

$$\varepsilon(E) = \frac{N_b(E)\Delta E}{\int_E^{E+dE} N(E)dE} \quad (3)$$

where $N_b(E)$ is the measured number of Bremsstrahlung photons emitted from a thick target at a given energy E, ΔE the energy channel width, and $N(E)dE$ the simulated Bremsstrahlung emission obtained from the general purpose MC code PENELOPE [21] for the same material in the energy interval [E:E+dE]. The width ΔE can be specified by the EDS software. To avoid the influence of characteristic peaks on the measured Bremsstrahlung, two thick targets were chosen: a silicon standard

for efficiency determination in the low energy region *200 eV ⩽ E ⩽600 eV,* and a carbon standard for energies *E >600 eV*.

Finally, the resulting spectrum was fitted by the Levenberg-Marquardt non-linear least square method, using the model of Castellano and Trincavelli for the generated Bremsstrahlung intensity [22]:

$$I_{bg}{}^{C-T}(E) = K\sqrt{Z}\left(\frac{(E_0 - E)}{E}\right)\left(a_1 + a_2E + a_3ln(Z) + a_4\frac{{E_0}^{a_5}}{Z}\right)\left[1 + (a_6 + a_7E_0)\frac{Z}{E}\right] \quad (4)$$

where K is a scaling factor, Z is the atomic number, E_0 is the incident electron energy (in keV) and a_i are parameters to fit. The expression given in equation (4) was proved to give more reliable background construction than other models, such as those of Small et al. [23] and Duncumb et al. [24]. The inputs in the fitting process are K and E_0. The value of K was *a priori* determined by fitting the Bremsstrahlung of a silicon thick target using equation (4). In this case, a_i were not fitting parameters and their values given in Castellano and Trincavelli's work [22] were used as inputs. For cases where Bremsstrahlung of the substrate had minor contribution to the measured background, Z of the particle was used as input in equation (4). Otherwise, Z was also a parameter to fit. A first version of the Bremsstrahlung model in equation (4) has already been shown to be suitable for the quantitative analysis of microparticles [14].

The Bremsstrahlung intensity ${I^i}_{bg}$ under the line associated with the element i can afterward be calculated as:

$${I^i}_{bg} = {I_{bg}}^{C-T}(E^i)\,\varepsilon(E^i)\,R(E^i)\,f(\chi^i) \quad (5)$$

where E^i is the energy corresponding to the line of the element *i*.

Correction of substrate effects. A phenomenon that influences the $\frac{P}{B}$ ratios when analyzing particles deposited on a substrate is the substrate emission. The transmission of electrons through the particle induces Bremsstrahlung from the substrate that contribute to the measured background, leading to incorrect $\frac{P}{B}$ ratios of the particle.

We can correct for the substrate emission by considering its contribution to the measured Bremsstrahlung emission:

$${I^i}_{bg} = {I^i}_{bg_{particle}} + {I^i}_{bg_{substrate}} \quad (6)$$

I^i_{bg} is the Bremsstrahlung intensity obtained from equation (5). Equation (4) includes many parameters that were adjusted to describe the Bremsstrahlung emission of bulk samples. For our purposes, the values of a_i proposed by Castellano and Trincavelli [22] did not provide accurate corrections when applied to small particles (see below, Fig. 5). Instead, the model suggested by Small et al. [23] was used. Considering absorption and backscattering effects in Small et al's model, we can write:

$${I_{bg}}^{Small}(E^i) = f(\chi^i)R(E^i)KZ^m\left(\frac{E_0 - E^i}{E^i}\right)^m \exp(B) \quad (7)$$

where $f(\chi)$ is the absorption factor and R is the backscattering correction for Bremsstrahlung calculated from equation (1). The last term describes the Bremsstrahlung generated intensity given by Small et al where $m = 0.00599E_0 + 1.05$ and $B = -0.0322E_0$.

Regarding the substrate emission, primary electrons are backscattered from both the particle and the substrate. Hence, two backscattering factors need to be included in equation (7). This is also the case for the absorption effects, since X-rays that are emitted from the substrate are absorbed inside

the substrate and inside the particle before reaching the detector. In addition, the Bremsstrahlung of the substrate needs to take into account the energy loss of electrons after crossing the particle. The remaining energy of electrons E_0' after exiting the particle can be approximated as [25]:

$$E_0' = E_0(1 - \frac{S}{Y})^{3/5} \qquad (8)$$

where S(μm) is the thickness of the particle and Y the Kanaya-Okayama electron range radius [25]. Equation (6) can now be expressed as:

$$I^i{}_{bg} = I^i{}_{bg_{particle}} \left(1 + \frac{(Z_{substrate})^{m'}}{(Z_{particle})^m} \times \frac{R_{subtrate}\, f(\chi)_{substrate} \left(\frac{E_0{}' - E^i}{E^i}\right)^{m'} \exp(B')}{\left(\frac{E_0 - E^i}{E^i}\right)^{m} \exp(B)} \right) \qquad (9)$$

where m', $\exp(B')$, $R_{subtrate}$ and $f(\chi)_{substrate}$ are calculated at E_0'.

There are, however some complications in the correction of substrate Bremsstrahlung that include determining the thickness S for particles with irregular shapes and evaluating the substrate emission induced by electrons that exit the particle through side scattering. In addition, calculating Y in equation (8) requires a prior knowledge of the composition of the sample. This can limit the use of equation (9) in quantitative procedures. Therefore, an approximate method was used that enables a calculation of the energy loss of electrons from the analysis of the characteristic emission of the substrate. The X-ray emission of the substrate can be used as a good indicator of the mean distance travelled by electrons, as well as the average energy loss of electrons before crossing the particle.

The method is based on determining the parameter C in the following equation :

$$E_0' = E_0 \left(1 - \frac{C}{{E_0}^{1.67}}\right)^{3/5} \qquad (10)$$

with

$$C = \frac{S\, Z^{0.89} \rho}{0.0276\, A} \qquad (11)$$

where ρ(g cm^{-3}) is the particle density and A the mean atomic mass (g).

The first step is to analyze the particle at different electron energies $E_{0_{j=1,2..n}}$ and to measure the X-ray intensity corresponding to the K line of the substrate in each case. The intensities are afterward normalized by the intensity obtained at one of the electron energies, e.g. the highest one E_{0_n}. This enables relative intensities that are independent of the absorption inside the particle to be obtained. The main parameters that are dependent on the relative intensities are the electron energy after crossing the particle and the absorption inside the substrate at E_0'. Thus, by using the equation of Cosslett and Green [26] for characteristic intensities $I \approx \left(\frac{E_0}{E}\ln\left(\frac{E_0}{E}\right) - \frac{E_0}{E} + 1\right)$, the relative intensities I_r as a function of E_0 can be fitted using the following formula:

$$I_r(E_0) = \frac{f\left(\chi, E_0^{'}\right)_{substrate}}{f\left(\chi, E_{0_n}^{'}\right)_{substrate}} \times \frac{\sigma_0 \left(E_0 \ln\left(\frac{E_0\, \sigma_0}{E_s}\right) - E_0 + \frac{E_s}{\sigma_0}\right)}{\sigma_{0_n} \left(E_{0_n} \ln\left(\frac{E_{0_n}\, \sigma_{0_n}}{E_s}\right) - E_{0_n} + \frac{E_s}{\sigma_{0_n}}\right)} \qquad (12)$$

where:

$$\sigma_0 = \left(1 - \frac{C}{{E_0}^{1.67}}\right)^{\frac{3}{5}}, \quad \sigma_{0_n} = \left(1 - \frac{C}{{E_{0_n}}^{1.67}}\right)^{\frac{3}{5}} \qquad (13)$$

E_s is the energy corresponding to the K line of the substrate, $f\left(\chi, E'_{0_j}\right)$ the absorption factor determined at the electron energy E'_{0_j}, and C is the parameter to fit.

The values of I_r at a given energy E_{0_j} are obtained from the ratio:

$$I_r(E_{0_\mathrm{j}}) = \frac{I_{s_\mathrm{j}}}{I_{s_\mathrm{n}}} \qquad (14)$$

with I_{s_j} the characteristic intensity of the K line of the substrate acquired at E_{0_j}. After introducing the value of C in equation (10), E'_0 can be determined and used in equation (9).

If seeking to determine the energy loss of transmitted electrons at a given initial energy E_{0_k}, it is recommended to work with n ($3 \leq n \leq 7$) different electron energies, with E_{0_k} being the medium value (see example in appendix, table A2). The deviation between electron energies should preferably be $\leq$ 1 keV, in order to obtain an interaction volume and a mean distance travelled by the electrons that are more or less similar to those at E_{0_k}.

The method based on equation (12) can also enable the determination of an approximate thickness of the particle if the composition is known. To do so, it is recommended to work with large values of electron energies in order to reduce the amount of side scattered electrons and obtain electron trajectory segments that are more parallel. The thickness can be further determined from equation (11) using the value of C obtained from equation (12). This can solve some problems in 2D electron microscopy imaging of particles, such as determining a 3D form factor for a given particle.

It is worth noting that for very small particles, equation (9) should also take into account the loss in Bremsstrahlung intensity due to transmission. This loss can to some degree be considered similar to the loss due to backscattering effects [13, 17]. It can be assumed that electrons which exit the particle through transmission are electrons that would have potentially contributed to the X-ray emission of the particle with an electron energy equal to E'_0. In this case, the loss due to transmission can be taken into account by introducing a Bremsstrahlung backscattering correction factor, calculated at the energy E'_0 of transmitted electrons, in which the backscattering coefficient η is replaced by the total transmission coefficient η_T. η_T can be expressed using the formula given by Kanaya and Okayama [25]:

$$\eta_T = \exp\left(-\frac{Q\,\frac{S}{Y}}{1-\frac{S}{Y}}\right) \qquad (15)$$

with $Q = 0.187\ Z^{2/3}$ and $\frac{S}{Y}$ replaced by $\frac{C}{{E_0}^{1.67}}$.

Correction of transmission effects. According to Newbury et al. [11] the difference between the emission inside a particle and inside a bulk can be accounted for using $\frac{P}{B}$ ratios, except for very small particles. This can be explained to a certain extent by the fact that in particles bigger than the X-ray generation range the intensities are mostly influenced by absorption, whereas for smaller particles, the intensities are also affected by the loss due to transmitted electrons. As suggested by Lábár and Török [13], the loss due to transmission could be corrected by considering the non-linear dependence of the $\frac{P}{B}$ ratio to the mass thickness. The ratio being inversely proportional to ${\rho_D}^{0.15}$, a similar correction was applied in this work as $\left(\frac{C}{{E_0}^{1.67}}\right)^{0.15}$.

We can now express the corrected $\frac{P}{B}$ ratio of the element *i* in the particle as:

$$\left(\frac{P}{B}^{corr}\right)^{i} = \left(\frac{C}{{E_0}^{1.67}}\right)^{0.15} \frac{I^i - {I^i}_{bg_{particle}}}{{I^i}_{bg_{particle}}} \qquad (16)$$

where I^i is the characteristic intensity emitted from the element *i*. ${I^i}_{bg_{particle}}$ is the Bremsstrahlung intensity of the element *i* in the particle, obtained from equation (9).

Quantitative procedure. The quantitative method used in this work is the Lábár and Török [13] approach where the concentration of the element *i* can be determined using the following $\frac{P}{B}$ **ZAF** method:

$$C^i = k^i \, Z_c \, R_c \, A_c \, F_c \qquad (17)$$

with

$$k^i = \left(\frac{P}{B}\right)^{i}_{sample} \Big/ \left(\frac{P}{B}\right)^{i}_{standard} \qquad (18)$$

Z_c, R_c, A_c and F_c are correction factors of atomic number, backscattering, absorption and fluorescence, respectively. The authors pointed out that the main effects are those associated with atomic number. Factors of absorption and backscattering are only second-order corrections and fluorescence effects were neglected in the model. For this article, we will refer to the quantitative method as **ZAF** $\frac{P}{B}^{corr}$ when corrected $\frac{P}{B}$ ratios are used in equation (17) and **ZAF** $\frac{P}{B}^{uncorr}$ when no correction is applied.

RESULTS AND DISCUSSION

In order to investigate the influence of size effects, experimental $\frac{P}{B}$ ratios were determined at various acceleration voltages for K411 glass particles deposited on an Al substrate. A particle of ~2 µm was compared to a pseudo-bulk particle of 25 µm where size effects are negligible. Since the $\frac{P}{B}$ ratios are quasi-independent of absorption path lengths, they can give a good understanding of how X-ray emission is affected by the size of the particle. Fig 1 shows the deviations in uncorrected $\frac{P}{B}$ ratios as the electron energy increases.

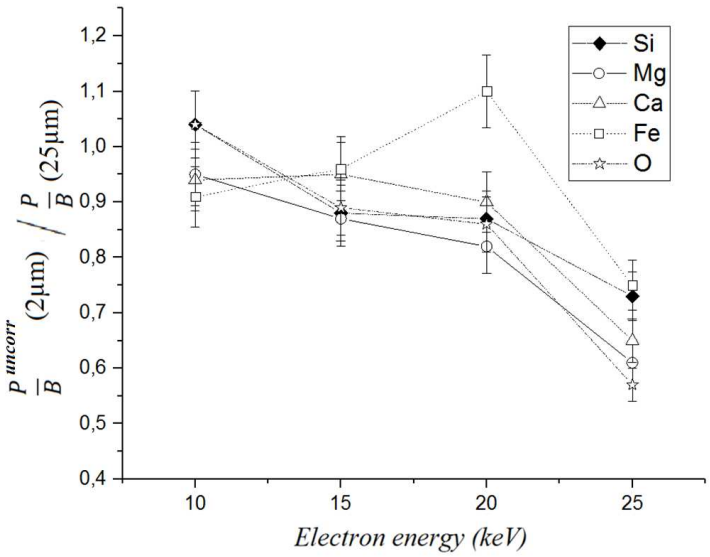

Fig. 1 Normalized uncorrected peak-to-background ratios of a 2 µm K411 glass particle on an Al substrate as a function of electron energy. The error bars represent standard deviations of measurements performed on 4 to 5 particles having the same diameter.

At E_0=10 keV, the X-ray generation volume is within the small particle volume and the deviations of uncorrected $\frac{P}{B}$ ratios from a bulk particle are less than 10%. The decrease of $\frac{P}{B}^{uncorr}$ (2 µm) becomes significant at 25 keV, which is mainly due to the contribution of the continuum radiation of the substrate to the measured background. If not taken into account, the substrate emission can lead to an overestimation of the Bremsstrahlung intensities and thus to lower ratios.

For 15 keV$\leq E_0 \leq$20 keV, the decrease due to the substrate emission in the $\frac{P}{B}^{uncorr}$ ratios of the particle is more or less compensated for by the transmission effects. In fact, Wendt [27,13] suggested that characteristic intensities increase with the mass thickness ρ_D as ${\rho_D}^{1.15}$, whereas Bremsstrahlung intensities are proportional to ${\rho_D}^{1.3}$. This results in $\frac{P}{B}$ ratios of small particles bigger than those of a bulk sample.

Another important parameter that should be considered when studying the influence of the substrate emission is the substrate atomic number. The contribution of the substrate to the measured Bremsstrahlung increases with its atomic number. We show in Fig 2 the measured Bremsstrahlung of a 2 µm glass particle deposited on W and B_4C substrates. It can be observed that the measured background becomes more important when a W substrate is used.

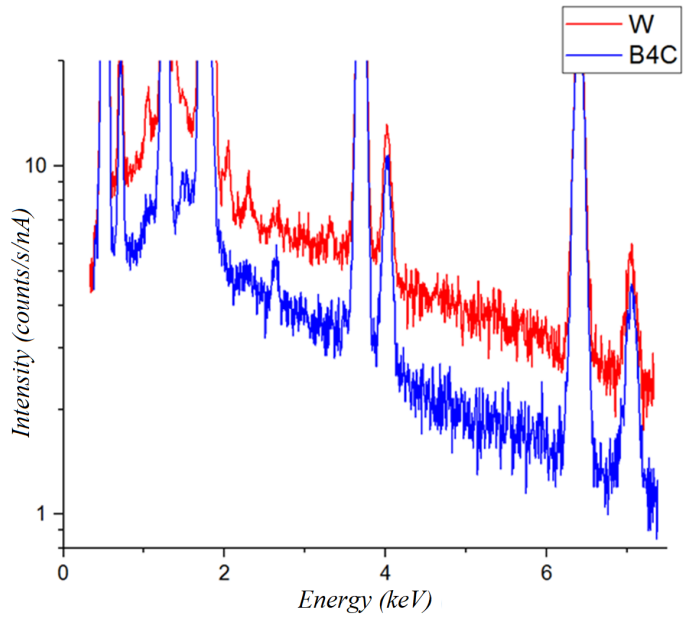

Fig. 2 Backgrounds of a 2 µm K411 spherical particle deposited on W and B_4C substrates.

The characteristic intensities of the particle deposited on a B_4C substrate did not differ significantly from those of a W substrate. Thus, secondary X-ray emission caused by the substrate radiation was ignored in our correction model.

In order to assess the validity of the substrate emission correction, the first step was to evaluate equation (12) and to determine the parameter C for particles with known thicknesses. Analyses were therefore performed on five different sizes of calibrated NIST K411 spherical particles, as shown in Fig 3.

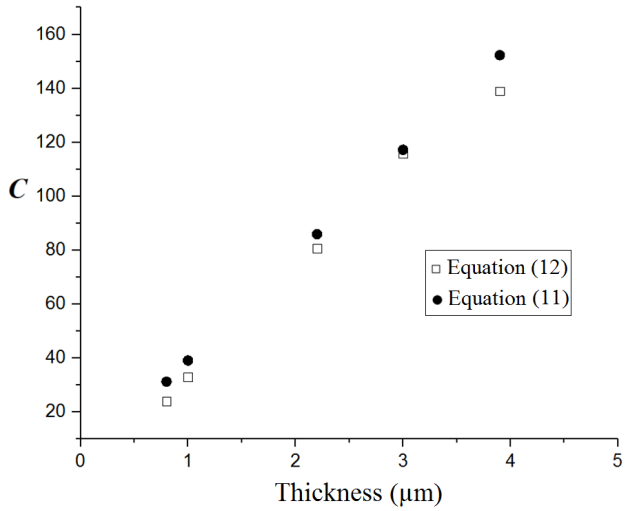

Fig. 3 Comparison between the values of C given by equation (11) and those obtained from the method based on equation (12) as a function of the thickness S.

It can be seen that the results obtained with equation (12) agree with the values of C given by equation (11). The deviations found probably result from electrons that exit the particle through side scattering. The distance travelled by these electrons is shorter than the diameter of the spherical particle. This led to a calculated value of C by equation (12) slightly smaller than the one obtained with equation (11) where S is set equal to the diameter. Nevertheless, estimating the energy loss of electrons through the substrate emission gives a more realistic description than if it is determined at a given depth where the electrons are assumed to undergo the same energy loss and strike the substrate at the same energy.

Bremsstrahlung emission was further analyzed at E_0=20 keV for the case of a 2.4 µm K411 particle deposited on four B_4C, Al, Ni, and W substrates. The experimental Bremsstrahlung intensities were determined from equation (5) and compared to results calculated by equation (9). The comparison was performed in terms of $\frac{I^i{}_{bg}(\mathrm{B4C})}{I^i{}_{bg}(\mathrm{W,Ni,Al})}$ ratios as shown in Fig 4.

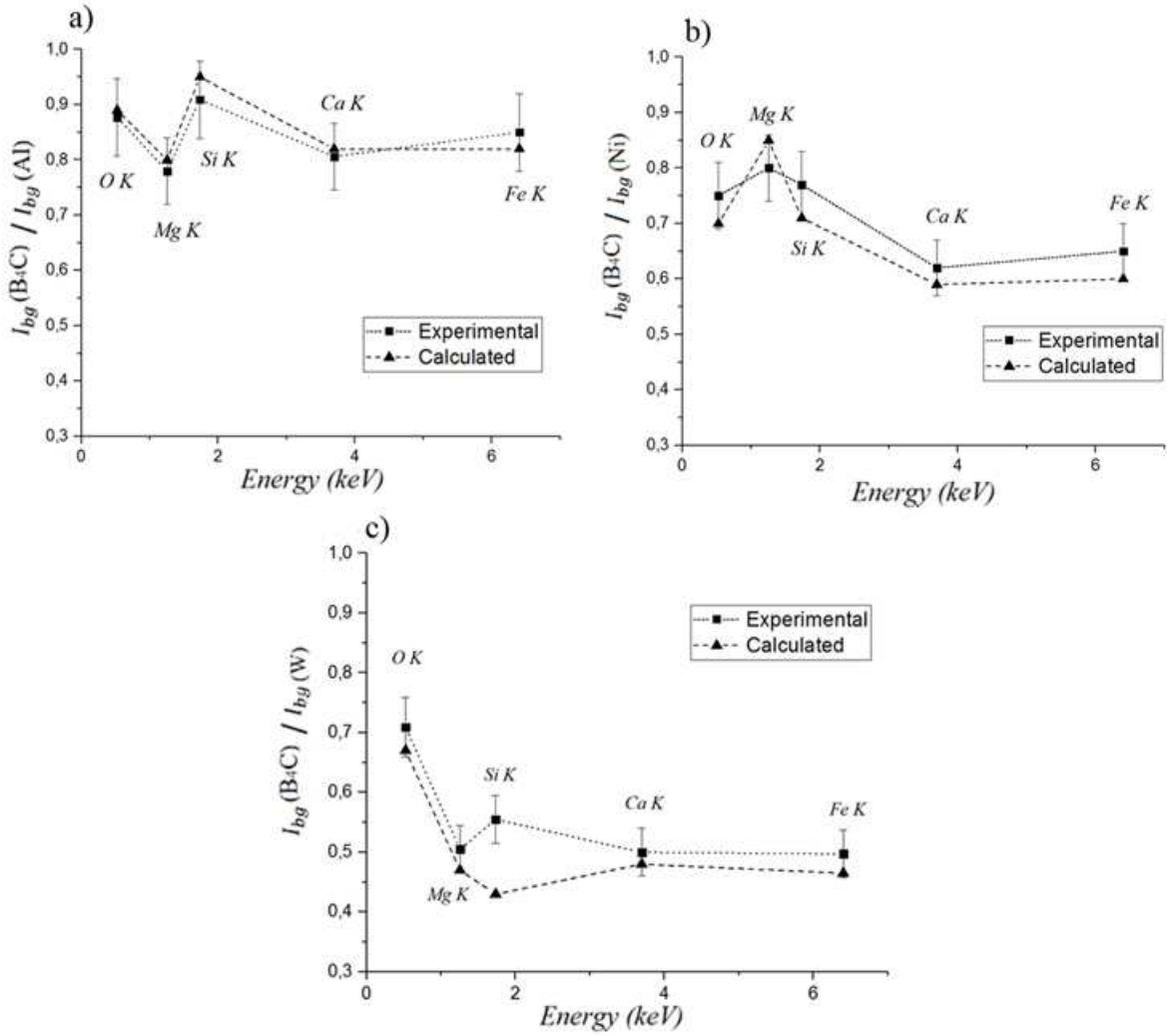

Fig. 4 Experimental and calculated contribution of the substrate to the measured background of a 2.4 µm K411 spherical particle deposited on Al (**a**), Ni (**b**), and W (**c**). The contribution of the substrate is evaluated in terms of $\frac{I^i{}_{bg}(B4C)}{I^i{}_{bg}(W,Ni,Al)}$. The error bars represent standard deviations of 5 to 6 measurements performed on one particle, each time a substrate is used.

It can be noticed that except for Si K in the case of a W substrate, equation (9) gives a good description of the substrate contribution, with calculated values falling within the range of experimental error bars. The deviations between averaged experimental values and calculated ones do not exceed 10%. The discrepancy seen in Fig 4c is probably due to the fact that W has an absorption edge at an energy of ~1810 eV, close to the Si Kα line, which results in reduced accuracy in the background construction model. The background of the substrate increases with the atomic number Z, which leads to a high contribution of the substrate to the measured background. At low energies, the emission of the substrate is constrained by absorption inside both the substrate and the particle.

It is important to note that the accuracy of the correction of substrate effects is also dependent on the Bremsstrahlung model used in equation (9). This is shown in Fig. 5 by comparing experimental values of $\frac{I^i{}_{bg}(\mathrm{B4C})}{I^i{}_{bg}(\mathrm{Ni})}$ for a 0.8 µm K411 spherical particle, to calculated ones using two different

Bremsstrahlung models. Good results were obtained when the contribution of the substrate is calculated from equation (9), which is based on the Small et al.'s model. The contribution of the Ni substrate to the measured background was underestimated when the Castellano and Trincavelli's model was applied, which led to an overestimation in the calculated $\frac{I^i{}_{bg}(\mathrm{B4C})}{I^i{}_{bg}(\mathrm{Ni})}$.

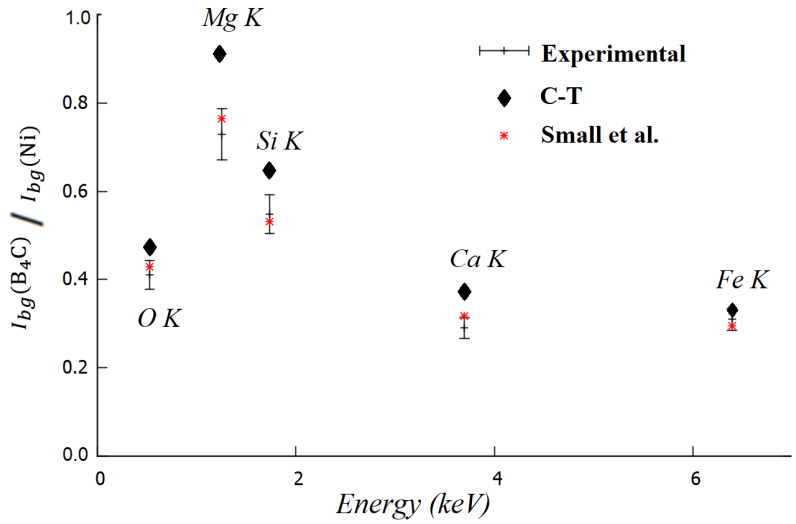

Fig. 5. Experimental and calculated $\frac{I^i{}_{bg}(B4C)}{I^i{}_{bg}(Ni)}$ of a 0.8 µm K411 spherical particle deposited on Ni and B_4C substrates. The contribution of the substrate is calculated from Castellano & Trincavelli (C-T) and Small et al. models. The error bars represent standard deviations of measurements performed on 5 particles having approximately the same diameter.

The effects of transmission were studied for two sizes (0.8 µm and 2.4 µm) of spherical K411 particles deposited on a Ni substrate. Table 1 presents the normalized $\frac{P}{B}$ ratios of the particle (i.e. $\frac{I^i - I^i{}_{bg_{particle}}}{I^i{}_{bg_{particle}}}$ divided by $\frac{P}{B}$ ratios of a pseudo-bulk particle) and corrected ones determined from equation (16). The Bremsstrahlung emission of the substrate was removed using equation (9).

Table 1. Normalized peak-to-background ratios $\tau = \frac{\frac{P}{B}(particle)}{\frac{P}{B}(\mathrm{pseudo-bulk})}$ for K411 spherical particles. $\frac{P}{B}$ ratios were obtained at E_0=20 keV. τ^{corr} stands for the normalized $\frac{P^{corr}}{B}$ determined from equation (16).

	$\tau(0.8\mu m)$	$\tau(2.4\mu m)$	$\tau^{corr}(0.8\mu m)$	$\tau^{corr}(2.4\mu m)$
O	1.36	1.03	1.03	0.94
Mg	1.18	1.05	0.89	0.96
Si	1.40	1.17	1.06	1.07
Ca	1.31	1.10	0.99	1.00
Fe	1.58	1.22	1.19	1.12

It can be seen that $\frac{P}{B}$ ratios increase for all elements as the size of the particle decreases. The deviations from a pseudo-bulk particle are considerable for the 0.8 µm particle, with $\tau =$

$\frac{\frac{P}{B}(particle)}{\frac{P}{B}(\text{pseudo}-\text{bulk})}$ increasing up to 1.58 for Fe. Similar results were obtained by Newbury et al. [11], where MC simulations were performed on spherical and cylindrical glass particles. The authors associated the effects of transmission on $\frac{P}{B}$ ratios with anisotropy in the Bremsstrahlung generation and the difference in the behavior of a cross section for continuum and characteristic radiations. By applying the necessary corrections, it can be observed that except for Fe, the variation of $\frac{P}{B}$ ratios with particle size becomes less significant, with deviations from the pseudo-bulk particle that do not exceed 11%. These deviations probably result from discrepancies in the background construction model, equation (9), and the method used for the correction of transmission effects.

In order to evaluate the correction models in terms of quantitative analysis, concentrations were calculated for the 0.8 µm K411 particle using equation (17). We show in table 2 the results obtained from using both corrected and uncorrected $\frac{P}{B}$ ratios as well as their deviations from nominal concentrations *Cn*. It must be noted that uncorrected $\frac{P}{B}$ ratios used for quantification are those determined directly from the X-ray spectrum of the particle (i.e. the substrate Bremsstrahlung was not removed from the measured background). The results presented in table 2 indicate clearly that using uncorrected $\frac{P}{B}$ ratios for quantitative analyses can lead to significant errors when size effects are pronounced. The concentrations of Ca and Fe were underestimated with deviations from nominal concentrations reaching up to 38% for Ca. On the other hand, accurate quantitative results were obtained from using corrected $\frac{P}{B}$ ratios and the deviations from nominal concentrations did not exceed 7%.

For the analysis of uranium oxide, studies were performed on a 0.9 µm spherical UO_2 particle and on an agglomerated UO_2 particle with an irregular shape, both deposited on an Al substrate. Fig 6 shows the comparison between the X-ray spectrum of the spherical particle and that obtained for a bulk sample. As expected, two important phenomena are observed in the case of the small particle, i.e. the significant emission of the Al substrate and its own X-ray emission that is affected by both absorption and size effects.

Table 2. Averaged calculated concentrations (*Cc*) and their standard deviations for a 0.8 µm spherical particle of K411 glass. The quantification was performed on 5 particles having approximately the same diameter (0.80 ± 0.02 µm). The particle composition is certified by the National Institute of Standards and Technology as *Cn*.%(O)=42.9±1.2, *Cn*.%(Mg)=9.2±1.4, *Cn*.%(Si)=25.6±1.7, *Cn*.%(Ca)=11.2±2.3 and *Cn*.%(Fe)=11.2±2.3. $\Delta C\ (\%) = \frac{|Cc-Cn|}{Cn} \times 100$ represents the deviation from nominal concentration *Cn*.

ZAF $\frac{P}{B}^{uncorr}$	O	Mg	Si	Ca	Fe
Cc (wt. %)	51.3±1.7	11.2±0.6	22.8±1.1	6.9±0.5	7.8±0.7
ΔC (%)	19.5	21.7	10.9	38.4	30.4
ZAF $\frac{P}{B}^{corr}$					
Cc (wt. %)	45.1±1.4	8.7±0.6	23.8±1.2	10.5±0.8	11.8±1.0
ΔC (%)	5.1	5.4	7.0	6.2	5.4

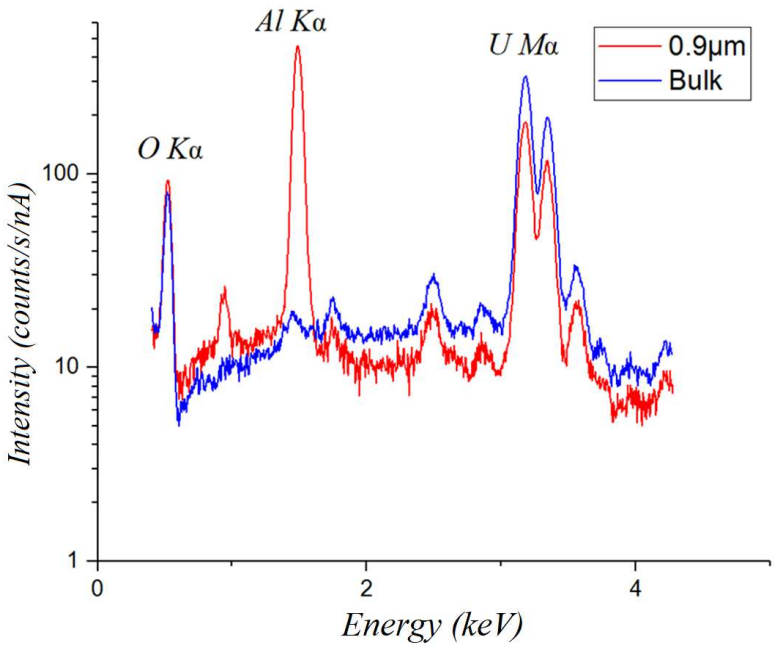

Fig. 6 X-ray spectrum of a 0.9 µm UO_2 spherical particle on an Al substrate compared to that obtained for a bulk sample.

At low energies, absorption has a considerable effect, leading to an X-ray intensity loss which is more prominent in the case of a bulk sample. As photon energies increase, absorption has less influence, and the intensity loss due to transmission effects is more pronounced. The contribution of the substrate to the measured background is less significant in this case, since $Z_{particle} >> Z_{substrate}$. No correction for substrate effects was therefore required in the analysis of UO_2 particles. The $\frac{P}{B}$ ratios of the spherical particle were further determined and compared to those of a bulk sample, as shown in table 3. The deviations between $\frac{P}{B}$ ratios of the particle and those of a bulk sample were found to be less than 10% even for uncorrected ratios. The small difference between uncorrected and bulk ratios is a direct consequence of the weak influence of the substrate emission on the measured background of the particle. In addition, corrected ratios were different from uncorrected ones by a factor of ~0.86, which indicates that electron transmission had only minor effects on the particle's $\frac{P}{B}$.

The agglomerated particle was later analyzed at an electron energy of 20 keV. The electron incidence point was randomly set at the position indicated by the red circle in Fig 7a. The energy loss of electrons at this position was estimated to be about 80%, corresponding to a thickness of ~0.8 µm. The X-ray spectrum measured at the red circle can give an idea as to whether the estimated thickness is reliable. Fig 7b illustrates the X-ray spectrum of the agglomerated particle and that of the 0.9 µm spherical particle, which show close X-ray intensity values. The deviations in characteristic intensities at the top of the peaks do not exceed 20%, whereas for Bremsstrahlung intensities under the peak the deviations range from 10 to 22%. As it is difficult to conclude as to where these deviations come from, but a probable explanation is that they result from the difference in absorption path lengths and in the surface shape of the two particles. On the other hand, this difference can be taken into account by using $\frac{P}{B}$ ratios, as shown in table 3. It can be observed that the deviations between all the ratios are not significant, which can be explained by both the weak influence of the substrate emission and the minor effects of electron transmission.

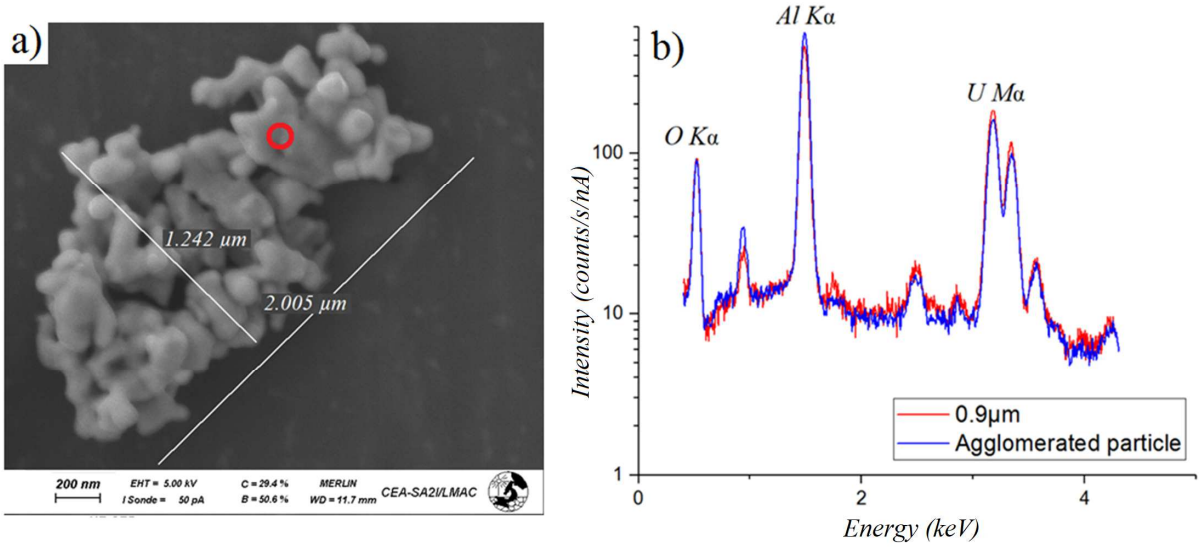

Fig. 7 a) Scanning electron microscopy image of the studied agglomerated UO2 particle. **b)** X-ray spectrum of a 0.9 µm spherical UO_2 particle on an Al substrate in comparison with that obtained for an agglomerated particle at a position (red circle in Fig 7a) corresponding to a thickness of about 0.8µm.

In order to identify the ratio deviations in terms of quantitative results, concentration were calculated for UO_2 particles using equation (17). We present in table 4, the calculated concentrations Cc for each particle as well as their deviations from nominal concentrations Cn. In comparison, results obtained by a conventional ZAF method are also presented.

Table 3. Comparison between uncorrected and corrected $\frac{P}{B}$ ratios of UO_2 particles as well as those obtained for a bulk sample. For particles, uncertainties are presented as the standard deviation of $\frac{P}{B}$ ratios determined from 4 to 6 measurements performed on each particle. For the bulk, uncertainties are evaluated from measurements of 5 different zones of the sample.

	U	O
$\frac{P^{uncorr}}{B}$ (0.9 µm)	23.1±0.7	7.3±0.3
$\frac{P^{corr}}{B}$ (0.9 µm)	19.9±0.6	6.3±0.3
$\frac{P^{uncorr}}{B}$ (agglomerated particle)	22.5±0.8	7.7±0.6
$\frac{P^{corr}}{B}$ (agglomerated particle)	19.1±0.7	6.5±0.5
$\frac{P}{B}$ (bulk)	21.1±0.8	6.8±0.3

Table 4. Average quantitative results *Cc* and their standard deviations obtained from equation (17) for particles of stoichiometric UO_2. Standard deviations represent uncertainties associated with the measurements described in table 3. $\Delta C\ (\%) = \frac{|Cc-Cn|}{Cn} \times 100$ represents the deviation from nominal concentration.

0.9 µm particle	Cc %(U)	ΔC (%)	Cc %(O)	ΔC (%)
Conventional ZAF	81.1±0.2	8.0	18.9±0.2	69.5
ZAF $\frac{P^{uncorr}}{B}$	88.4±0.8	0.3	11.6±0.8	2.1
ZAF $\frac{P^{corr}}{B}$	88.3±0.8	0.2	11.7±0.8	1.3
Agglomerated particle				
Conventional ZAF	78.2±0.3	11.3	21.8±0.3	84.0
ZAF $\frac{P^{uncorr}}{B}$	87.4±0.7	0.9	12.6±0.7	6.3
ZAF $\frac{P^{corr}}{B}$	87.5±0.7	0.7	12.5±0.7	5.4

As expected, the weak deviations between the particle's $\frac{P}{B}$ ratios and those of the bulk resulted in a negligible difference between the calculated concentrations. This suggests that a correction step is only necessary in cases where substrate and transmission effects are prominent. Nevertheless, using a $\frac{P}{B}$ method for standard based quantification of microparticles is essential. As shown in table 4, equation (17) provided accurate quantitative results with deviations from *Cn* that did not exceed 7%. On the other hand, inaccurate results were obtained by using the conventional ZAF method and the deviations between *Cc* and *Cn* reached up to 84% for O in the agglomerated particle. Conventional methods do not account for the difference in absorption between particles and the bulk, or for transmission effects. It is worth reminding that even though the transmission of electrons through the particle had minor effects on the $\frac{P}{B}$ ratios, it had a significant impact on the characteristic intensities, especially at high energies (Fig. 6). Without correcting for these effects, conventional quantitative methods where characteristic intensities are used can lead to large errors.

CONCLUSION

Correction for X-ray intensity loss in small sized particles was achieved using a peak-to-background method. Two important effects can be identified in the analysis of microparticles, i.e. absorption and size effects. With $\frac{P}{B}$ ratios being almost independent of absorption path lengths, a correction model for size effects has been proposed enabling the influence of both transmission effects and substrate emission to be taken into account. Inaccuracies in the correction model could be due to detector efficiency determination, uncertainties in mass absorption coefficients at low energies and the different empirical formulas used in this work.

The correction for size effects in microparticles depends on the estimation of the energy loss of transmitted electrons. This requires a prior knowledge of the distance that electrons travel inside the particle, which often seems very complicated to obtain. The method based on equation (12) enables such a difficulty to be dealt with, and can serve in the determination of an approximate thickness for particles with undefined geometry.

For K411 glass particles, $\frac{P}{B}$ ratios were significantly affected by both the substrate emission and electron transmission, which led to inaccurate results when a $\frac{P}{B}$ method was used for quantitative analysis. After correcting for size effects, significant improvements were obtained in terms of quantitative results with deviations from nominal concentrations that did not exceed 7%. In the case of UO_2 particles, size effects did not have much impact on $\frac{P}{B}$ ratios and accurate quantitative results were obtained from both corrected and uncorrected ratios.

Although the approach described here only concerned the case of individual microparticles, it has the potential to be applied to the correction of size effects in microparticle assemblies with unusual shapes. This therefore opens up the possibility of performing quantitative analyses of industrial powders, such as catalyst pellets or geological sample powders for energy production and environmental purposes.

Corresponding Author

*E-mail: mouad.essani@cea.fr

ACKNOWLEDGMENTS

We acknowledge the financial support received from the Cross-Disciplinary Program on Instrumentation and Detection of the CEA, the French Alternative Energies and Atomic Energy Commission. We are grateful to Dr P. Jonnard from the LCPMR laboratory at Sorbonne Université for reviewing this article so attentively. We also thank Dr N. Clavier from ICSM/LIME laboratory at the CEA for providing us with spherical uranium oxide microparticles.

Conflicts of interest: The authors declare no competing financial interest

REFERENCES

[1] J. Philibert, L'Analyse quantitative en microanalyse par sonde électronique. Métaux, Corrosion. Industrie 40 (1964), 157,216,325.

[2] J.L. Pouchou, F. Pichoir, Quantitative analysis of homogeneous or stratified microvolumes applying the model “PAP”, in: K.F.J. Heinrich, D.E. Newbury (Eds.), Electron Probe Quantitation, Plenum Press, New York, USA, (1991), pp. 31–76.

[3] L. Sorbier, E. Rosenberg E, C .Merlet, Microanalysis of porous materials, Microsc. Microanal. 10 (2004), 745-752. https://doi.org/10.1017/S1431927604040681

[4] C.E. Taylor, S.D. Garvey, J.E Pemberton, Carbon contamination at silver surfaces: surface preparation procedures evaluated by Raman spectroscopy and X-ray photoelectron spectroscopy, Anal. Chem. 68 (1996) 2401-2408. https://doi.org/10.1021/ac950753h.

[5] M.C.O. Mariana, M.T.M. Koper, Alumina contamination through polishing and its effect on hydrogen evolution on gold electrodes, Electrochimica Acta. 325 (2019) 134915. https://doi.org/10.1016/j.electacta.2019.134915.

[6] J.T. Armstrong, Quantitative elemental analysis of individual microparticles with electron beam instruments. in: K.F.J. Heinrich, D.E. Newbury (Eds.), Electron Probe Quantitation, Plenum Press, New York, USA, (1991) 261-315.

[7] I. Szalóki, J. Osán , C-U. Ro, R. Van Grieken, Quantitative characterization of individual aerosol particles by thin-window electron probe microanalysis combined with iterative simulation Spectrochim Acta Part B. 55 (2000) 1017-1030. https://doi.org/10.1016/S0584-8547(00)00174-9.

[8] M. Choël, K. Deboudt, P. Flament, Evaluation of quantitative procedures for X-ray microanalysis of environmental particles, Microsc. Res. Tech. 70 (2007). 996-1002. https://doi.org/10.1002/jemt.20510.

[9] D.E. Newbury, Quantitative electron probe microanalysis of rough targets: Testing the peak-to-local background method, Scanning. 26 (2004) 103-114. https://doi.org/10.1002/sca.4950260302.

[10] P.J. Statham, Use of spectrum simulation to predict detection limits and improve confidence in x-ray analysis. in: D.B. Williams, R. Shimizu (Eds), Proceedings of the 2nd Conference of International Union of Microbeam Analysis Societies. Bristol, UK: Institute of Physics Conference Series No. 165 (2000) 415–416.

[11] D.E. Newbury, K.F.J. Heinrich, R.L. Myklebust, J.A. Small, Monte Carlo electron trajectory simulation-an aid for particle analysis, National bureau of standards Spec Pub. 533. (1980) p. 39.

[12] J. Heckel, P. Jugelt, Quantitative analysis of bulk samples without standards by using peak-to-background ratios, X-Ray Spectrom. 13 (1984) 159–165. https://doi.org/10.1002/xrs.1300130407.
[13] J. Lábár, S. Török, A peak-to-background method for electron probe X-ray microanalysis applied to individual small particles, X-Ray Spectrom. 21 (1992) 183–190. https://doi.org/10.1002/xrs.1300210407.
[14] J. Trincavelli, G. Castellano, J. Riveros, Model for the bremsstrahlung spectrum in EPMA. Application to standardless quantification, X-Ray Spectrom. 27 (1998) 81–86. https://doi.org/10.1002/(SICI)1097-4539(199803/04)27:2<81::AID-XRS253>3.0.CO;2-R.
[15] K.F.J. Heinrich, H. Yakowitz, Absorption of primary x-rays in electron probe microanalysis, Anal. Chem. 47 (1975) 2408–2411. https://doi.org/10.1021/ac60364a018.
[16] B.L. Henke, E.M. Gullikson, J.C. Davis, X-ray interactions: photoabsorption, scattering, transmission and reflection at 50–30,000 eV, Z = 1-92, At. Data Nucl. Data Tables 54 (1993) 181–342. https://doi.org/10.1006/adnd.1993.1013.
[17] P.J. Statham, in: D.E. Newbury (Ed.), A ZAF Procedure for Microprobe Analysis Based on Measurement of peak-to-background ratios, Microbeam Analysis, San Francisco Press (1979) p. 247.
[18] G. Love, V.D. Scott, Evaluation of a new correction procedure for quantitative electron probe microanalysis (1978). J. Phys. D: Appl. Phys. 11, 1369.
[19] M. Alvisi, M. Blome, M. Griepentrog, V.D. Hodoroaba, P. Karduck, M. Mostert, M. Nacucchi, M. Procop, M. Rohde, F. Scholze, P. Statham, R. Terborg, J.F. Thiot, The determination of the efficiency of energy dispersive X-ray spectrometers by a new reference material, Microsc. Microanal. 12 (2006) 406–415. https://doi.org/10.1017/s1431927606060557.
[20] C. Merlet, X. Llovet, F. Salvat, Near-threshold absolute M-shell x-ray production cross sections of Au and Bi by electron impact, Phys. Rev. A: At. Mol. Opt. Phys. 78 (2008) 1–7 (022704). https://doi.org /10.1103/PhysRevA.78.022704
[21] F. Salvat, J.M. Fernández-Varea, J. Sempau. J. PENELOPE-2011: A Code System for Monte Carlo Simulation of Electron and Photon Transport, (2011); OECD/NEA Data Bank, Issy-les-Moulineaux, France.
[22] J. Trincavelli, G. Castellano, The prediction of thick target electron bremsstrahlung spectra in the 0.25–50 keV energy range, Spectrochim Acta Part B. 63 (2008) 1–8. https://doi.org/10.1016/j.sab.2007.11.009
[23] J. Small, S. Leigh, D. Newbury, R. Myklebust, Modeling of the bremsstrahlung radiation produced in pure-element targets by 10–40 keV electrons, J. Appl. Phys. 61 (1987) 459–469. https://doi.org/10.1063/1.338245.
[24] P. Duncumb, I.R. Barkshire, P.J. Statham, Improved X-ray spectrum simulation for electron microprobe analysis, Micros. Microanal. 7 (2001) 341–355. https://doi.org/10.1007/S10005-001-0010-6.
[25] K. Kanaya, S. Okayama, Penetration and energy-loss theory of electrons in solid targets, J. Phys. D :Appl. Phys. 5 (1972) p 43.
[26 M. Green, V.E. Cosslett, The efficiency of production of characteristic X-radiation in thick targets of a pure element Proc. Phys. Soc. 78 (1961) 1206.
[27] M. Wendt, Mikroanalyse dünner Schichten und Schichtstrukturen, Martin-Luther Universität Halle-Wittenberg Wissenschaftliche Beitrage (1984).

APPENDIX

A worked-through example is presented in this appendix where the correction of transmission and substrate effects is applied on peak-to-background ratios of a K411 spherical particle deposited on an Al substrate.

1-Determination of Bremsstrahlung intensities.

The fist step in determining Bremsstrahlung intensities consists on removing all the peaks from the measured spectrum as shown in Fig. A1 for the case of a 2.2 µm K411 spherical particle deposited on an Al substrate.

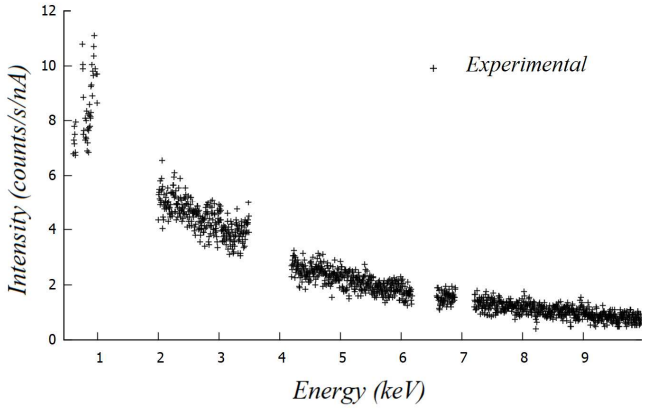

Fig. A1. *Background of a 2.2 µm K411 spherical particle deposited on an Al substrate, measured at an electron energy E_0 = 20 keV*

The resulting background should afterward be corrected for absorption, Backscattering effects and detection efficiency. The aim of this correction step is to obtain a shape of the curve that could be fitted with a model that describes the generated Bremsstrahlung intensity. After dividing the measured Bremsstrahlung intensities by absorption factor $\boldsymbol{f(\chi)}$, backscattering factor $\boldsymbol{R}$ and detector efficiency $\boldsymbol{\varepsilon}$, the resulting spectrum can be fitted using a model that describes the Bremsstrahlung generated intensities. The model of Trincavelli and Castellano (C-T) was applied to this end:

$$I_{bg}{}^{C-T}(E) = K\sqrt{Z}\left(\frac{(E_0 - E)}{E}\right)\left(a_1 + a_2E + a_3ln(Z) + a_4\frac{E_0{}^{a_5}}{Z}\right)\left[1 + (a_6 + a_7E_0)\frac{Z}{E}\right] \quad (A1)$$

Fig. A2. shows the corrected *Bremsstrahlung* intensities of the 2.2 µm K411 spherical particle as well as their fit using equation (A1).

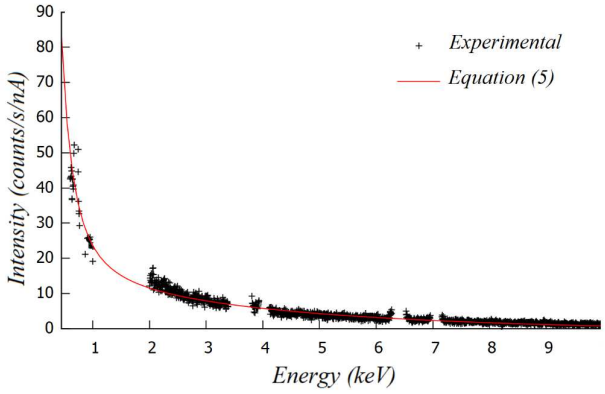

Fig A2. *Corrected Bremsstrahlung intensities of the 2.2 µm spherical particle fitted using equation (A1).*

The Bremsstrahlung intensity $I^i{}_{bg}$ under the line associated with the element i can afterward be calculated as:

$$I^i{}_{bg} = I_{bg}{}^{C-T}(E^i)\,\varepsilon(E^i)\,R(E^i)\,f^i(\chi^i) \quad (A2)$$

where E^i is the energy corresponding to the line of the element i. For the example shown in figure A2, the values of $I^i{}_{bg}$ obtained from equation (A2) are presented in table A1.

Table A1. Values of $I^i{}_{bg}$ obtained from equation (A2) for a 2.2 µm spherical particle deposited on an Al substrate.

Elements	O	Mg	Si	Ca	Fe
$E^i(keV)$-K line	0.52	1.25	1.74	3.69	6.39
$I^i{}_{bg}$ (counts/s/nA)	5.81	10.10	6.48	3.97	2.01

2-Correction of substrate effects.

The measured ${I^i}_{bg}$ shown in table A1 contain both the particle and the substrate Bremsstrahlung. In order to derive the Bremsstrahlung intensity emitted from the particle ${I^i}_{bg_{particle}}$, the following equation can be used:

$$ {I^i}_{bg_{particle}} = \frac{{I^i}_{bg}}{{F_s}^i} \qquad (A3) $$

with I^i_{bg} the Bremsstrahlung intensity obtained from equation (A2). ${F_s}^i$ is given by:

$$ {F_s}^i = \left(1 + \frac{(Z_{substrate})^{m'}}{(Z_{particle})^m} \times \frac{R_{subtrate}\, f(\chi)_{substrate} \left(\frac{{E_0}' - E^i}{E^i}\right)^{m'} \exp(B')}{R(E_0', \eta_T) \left(\frac{E_0 - E^i}{E^i}\right)^{m} \exp(B)} \right) \qquad (A4) $$

with $m = 0.00599E_0 + 1.05$ and $B = -0.0322E_0$. E_0' is the remaining energy of electrons after crossing the particle. $R(E_0', \eta_T)$ is the transmission factor with η_T the total transmission coefficient. E_0' can be obtained from the following equation:

$$ E_0' = E_0 \left(1 - \frac{C}{{E_0}^{1.67}} \right)^{3/5} \qquad (A5) $$

with

$$ C = \frac{S\, Z^{0.89} \rho}{0.0276\, A} \qquad (A6) $$

where ρ(g cm^{-3}) is the particle density and A the mean atomic mass (g).

The parameter C can be determined from the X-ray emission of the substrate on which the particle is deposited. The first step is to analyze the particle at different electron energies $E_{0_{\mathrm{j=1,2..n}}}$ and to measure the X-ray intensity I_s corresponding to the K line of the substrate in each case. The intensities are afterward normalized by the intensity obtained at one of the electron energies, e.g. the highest one $E_{0_{\mathrm{n}}}$. This enables relative intensities that are independent of the absorption inside the particle to be obtained. If seeking to determine the energy E_0' corresponding to a given initial energy $E_{0_{\mathrm{k}}}$, it is recommended to work with n ($3 \leq n \leq 7$) different electron energies, with $E_{0_{\mathrm{k}}}$ being the medium value. The deviation between electron energies should preferably be $\leq$ 1 keV. The relative intensities I_r are given by:

$$ I_r(E_{0_j}) = \frac{I_{s_{\mathrm{j}}}}{I_{s_{\mathrm{n}}}} \qquad (A7) $$

with $I_{s_{\mathrm{j}}}$ the characteristic intensity of the K line of the substrate acquired at $E_{0_{\mathrm{j}}}$ ($I_{s_{\mathrm{n}}}$ the substrate intensity corresponding to $E_{0_{\mathrm{n}}}$). Table A2 shows the values of I_r obtained from measuring $I_{s_{\mathrm{j}}}$ of the Al substrate after analyzing the 2.2 µm spherical particle at six different energies $E_{0_{\mathrm{j=1,2..6}}}$. In this example, E_0' was determined for an initial energy of 20 keV. The medium value was therefore set to $E_{0_{\mathrm{k}}}$=20 keV and the highest value of energies E_{0_6} was set equal to 23 keV.

Table A2. The values of I_r obtained from equation (A7) by analyzing a 2.2 µm spherical particle deposited on an Al substrate. Six electron energies were used: E_{0_1}= 18 keV, E_{0_2}= 19 keV… E_{0_5}= 22 keV with E_{0_6} = 23 keV the highest value used for normalization.

E_{0_j}(keV)	18	19	20	21	22
I_r	0.35	0.44	0.55	0.70	0.85

The second step consists on fitting the values of I_r as a function of E_{0_j} using the following formula:

$$I_r(E_0) = \frac{f\left(\chi, E_0^{'}\right)_{substrate}}{f\left(\chi, E_{0\mathrm{n}}^{'}\right)_{substrate}} \times \frac{\sigma_0 \left(E_0 \ln\left(\frac{E_0\,\sigma_0}{E_s}\right) - E_0 + \frac{E_s}{\sigma_0}\right)}{\sigma_{0\mathrm{n}} \left(E_{0_n} \ln\left(\frac{E_{0_n}\,\sigma_{0\mathrm{n}}}{E_s}\right) - E_{0\mathrm{n}} + \frac{E_s}{\sigma_{0\mathrm{n}}}\right)} \qquad (A8)$$

where:

$$\sigma_0 = \left(1 - \frac{C}{{E_0}^{1.67}}\right)^{\frac{3}{5}}, \quad \sigma_{0_n} = \left(1 - \frac{C}{{E_{0_n}}^{1.67}}\right)^{\frac{3}{5}} \qquad (A9)$$

E_s is the energy corresponding to the K line of the substrate, $f\left(\chi, E'_{0_j}\right)$ the absorption factor determined at the electron energy E'_{0_j}, and C is the parameter to fit. E_0 is the variable in equation (A8). Figure A3 shows the fit of I_r values presented in Table A2. A value of C=84.07 was obtained.

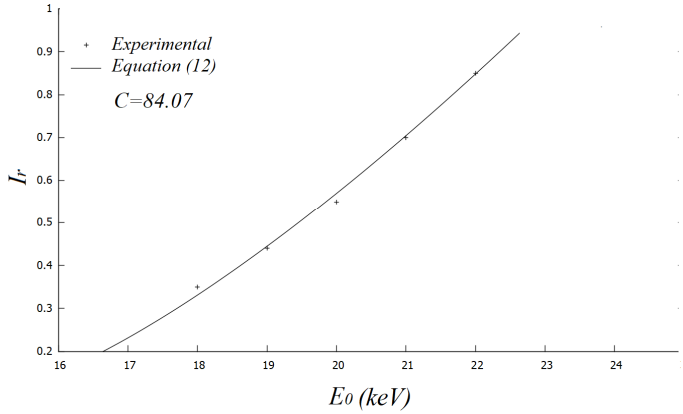

***Figure 3**. Relative intensities I_r fitted using equation (A8) with C the parameter to fit.*

After introducing the value of C in equation (A5), E'_0 can be determined and used in equation (A4). The method based on equation (A8) can also enable the determination of an approximate thickness of the particle if the composition is known. For instance, using a value of C=84.07 in equation (A6) gives a thickness S of about 2.16 µm which is in excellent agreement with the real value (the density of K411 glass is ρ = 2.946 g cm^{-3}).
η_T can afterward be determined from C using the following equation:

$$\eta_T = \exp\left(-\frac{Q\,\frac{C}{{E_0}^{1.67}}}{1 - \frac{C}{{E_0}^{1.67}}}\right) \qquad (A10)$$

with $Q = 0.187\,Z^{2/3}$. The transmission factor $R(E'_0, \eta_T)$ in equation (A4) can be further calculated from the backscattering factor R in which E'_0 is used instead of E_0, and the backscattering coefficient η is replaced by the total transmission coefficient η_T. Table A3 shows the values of ${I^i}_{bg_{particle}}$ of the 2.2 µm K411 particle obtained from equation (A3).

Table A3. Values of ${I^i}_{bg_{particle}}$ obtained from equation (A3) for a 2.2 µm spherical particle deposited on an Al substrate.

Elements	O	Mg	Si	Ca	Fe
$E^i(keV)$-K line	0.52	1.25	1.74	3.69	6.39
${I^i}_{bg_{particle}}$ (counts/s/nA)	5.01	6.77	5.21	2.66	1.42

3-Correction of transmission effects.

The intensity loss due to transmission effects could be corrected by multiplying the $\frac{P}{B}$ ratios of the particle to the factor $\left(\frac{C}{{E_0}^{1.67}}\right)^{0.15}$. The corrected $\frac{P}{B}$ ratio of the element *i* in the particle are expressed as:

$$\left(\frac{P^{corr}}{B}\right)^{i} = \left(\frac{C}{{E_0}^{1.67}}\right)^{0.15} \frac{I^{i} - {I^{i}}_{bg_{particle}}}{{I^{i}}_{bg_{particle}}} \qquad (A11)$$

where I^i is the characteristic intensity emitted from the element *i*. Table A4 shows the values of $\left(\frac{P^{corr}}{B}\right)^{i}$ of the 2.2 µm K411 particle obtained from equation (A11). In comparison, the $\frac{P}{B}$ ratio of a pseudo-bulk K411 particle, where size effects are negligible, are also presented.

Table A4. Comparison between corrected peak-to-background ratios $\left(\frac{P^{corr}}{B}\right)^{i}$ of a 2.2 µm spherical particle deposited on an Al substrate and those of a K411 pseudo-bulk particle.

Elements	O	Mg	Si	Ca	Fe
$E^i(keV)$-K line	0.52	1.25	1.74	3.69	6.39
$\left(\frac{P^{corr}}{B}\right)^{i}$	53.36	16.06	60.02	22.94	15.92
$\left(\frac{P^{pseudo-bulk}}{B}\right)^{i}$	61.07	17.20	63.47	20.16	14.65

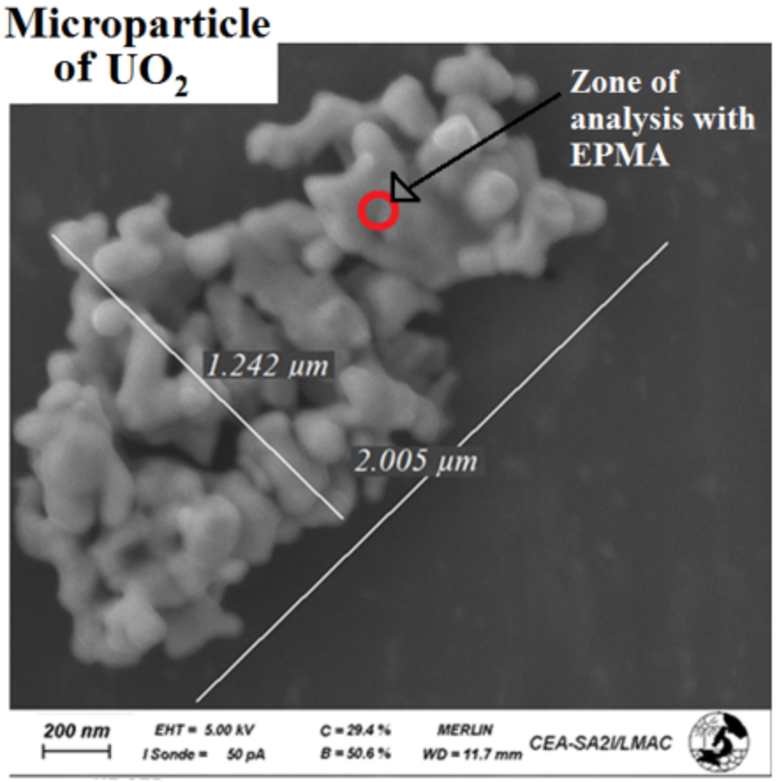

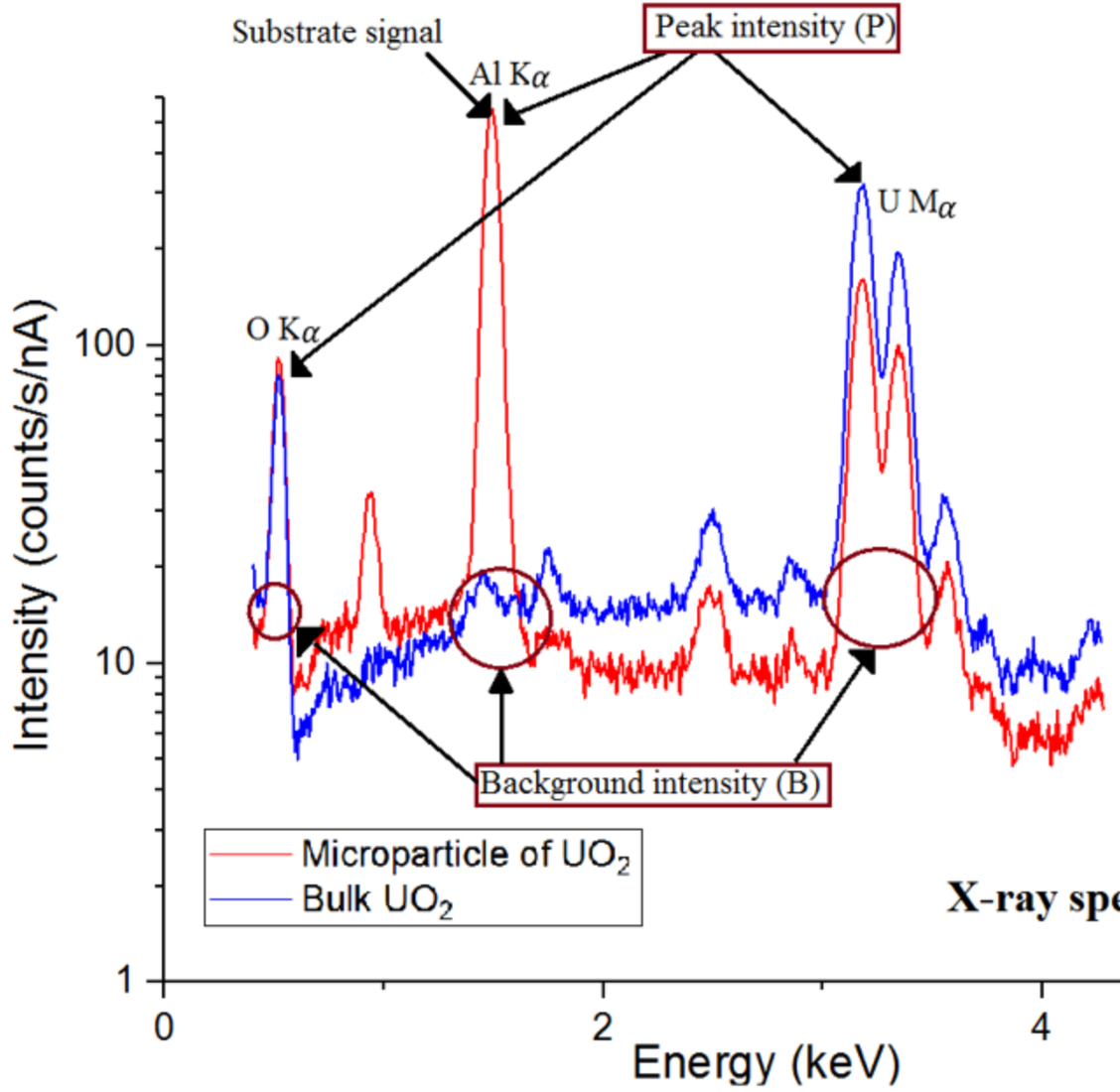

Peak intensity (counts/s/nA)

	U	O
P (Microparticle of UO_2)	161.1±3.2	91.3±4.8
P (Bulk UO_2)	320.1±17.3	80.8±1.3

Correction of size effects

Peak to background ratio

	U	O
$\frac{P}{B}$ (Microparticle of UO_2)	19.1±0.7	6.5±0.5
$\frac{P}{B}$ (Bulk UO_2)	21.1±0.8	6.8±0.3